Damage Mechanics of Microelectronics Solder Joints Under Concurrent Vibration and Thermal Loading

Basaran[1], **C., Zhao**[2], **Y.,** and **Cartwright**[3], **A.,**

[1] Assoc. Prof. and Director, [3] Assoc. Prof., and Co-Director

UB Electronic Packaging Laboratory, University at Buffalo, New York

[2] Senior Reliability Engineer, Analog Devices, Norwood, MA

cjb@eng.buffalo.edu

Abstract

Concurrent vibration and thermal loading is commonly encountered in the service life of electronic packaging, such as in automotive, airplane, military and mobile electronic devices. Solder joint reliability has been a critical issue of the overall design of microelectronic devices. However, the contribution of vibration to thermal fatigue life of solder joints has rarely been investigated. Presently, vibration is taken as a loading case that only causes elastic material response. Literature is scarce on vibration plasticity and vibration caused fatigue for micron scale structures. The standard practice in the industry is to use Miner's rule to calculate combined environment fatigue life. This study shows that using Miner's rule for fatigue life under combined loading is inaccurate for micron scale solder joints. There are a number of constitutive models to simulate thermomechanical behavior of solder joints, yet few of these, if any, models are verified by test data obtained from actual microelectronics solder joints. The authors see the need of such tests for the purpose of better understanding of material behavior of micron scale solder joints under thermal and vibration loading and providing a solid basis for more accurate material modeling and fatigue life prediction. This paper reports observations from a series of concurrent thermal cycling and vibration tests on 63Sn/37Pb solder joints of an actual ball grid array (BGA) package. Moiré interferometry (MI) is used to measure the inelastic deformation field of solder joints with submicron resolution. A large capacity Super AGREE thermal chamber and a high acceleration electrodynamic shaker are assembled together to

perform the concurrent cycling. The cyclic plasticity of solder joints and microstructure evolution are discussed and related to fatigue life prediction. The results obtained in this study agree with findings reported in the literature from micron scale material testing where it has been shown that “smaller is stronger,”

Keywords: concurrent cycling, Moiré interferometry, thermal cycling, vibration, fatigue life, inelastic behavior, BGA package, cyclic stabilization, damage evolution.

Introduction

Solder joint reliability has been an important issue in the electronic packaging industry. Technologies such as deep submicron VLSI design put millions of transistors in a single chip. Power density is ever increasing. Fine-pitch solder joints become common, and BGA solder joints tend to be one of the solutions for densely populated semiconductor devices. On the other hand solder joint reliability and fatigue life prediction still need to be developed and refined for the overall design of electronic devices for high performance and cost efficiency. As [1]Steinberg (1988) addressed: "Solder is so important in this process that many people in the industry claim that the reliability of the electronic equipment amounts to the reliability of the solder joints".

It is well known that the dominant failure mode for solder joints is low cycle thermal fatigue. This is caused by the thermal cycling of semiconductor devices and the coefficient of thermal expansion mismatch between the soldered layers ([2]Lau and Rice, 1985). The literature is scarce on the subject of the contribution of vibration damage to the overall fatigue life of solder joints. The common opinion is that vibrations only cause elastic material response ([3]Blanks 1976, [4]Markstein 1987, [5]Suhir and Lee 1988, [6]Barker and Sidhart 1995, [7]Darbha et al. 1996). [8]Upadhyayula and Dasgupta (1997) conducted highly accelerated stress test (HAST) on circuit card assemblies with surface mount components. Their test results

revealed that vibration loading at room temperature could sometimes be more damaging than similar vibration combined with thermal loading due to creep fatigue interaction. For example, one of their tests show that specimen under combined repetitive shock vibration (RSV) has longer fatigue life than similar RVS at room temperature. [9]Chandaroy and Basaran (1999) demonstrated that vibration could be an important failure cause. Their numerical simulations showed that viscoplasticity and creep of eutectic solder joints under vibration couldn't be ignored due to their low homologous temperature. Linear damage superposition rule (Miner's rule) is used in practice as a first order approximation for damage calculation and fatigue life prediction for concurrent loading case ([10]Barker et al. 1990, [11]Basaran and Chandaroy 1998). Miner's rule ignores the thermal and vibration interaction, and material microstructure and material property evolution, and size effect.

Much effort has been paid to modeling and simulating solder material. However, most of the models are based on test data obtained from bulk solder specimens under mechanical loading such as ([12]Busso et al. 1992, [13]Skipor et al. 1996, [27]Wei et al 1999). It is well known that bulk material behavior and properties are very different than micron scale materials ([14]Bonda and Noyan 1996, [19]Zhao et. al 1999). Highly accelerated stress test (HAST) is the standard method used in the industry. However, such tests usually do not provide information on stress strain relationship and quantitative mechanical behavior. As people begin to realize the size effect and the inaccuracy that results from using bulk material test data to calibrate model parameters, few tests have been done on solder joints of realistic packages. There are very few test data on actual size microelectronics solder joints. The lack of data is partially due to the difficulty in measuring the strain of solder joints sized under 0.5mm. Furthermore, conventional test conditions such as tension and shear cannot represent actual thermal cycling and vibration coupled with thermal cycling. Thermal vibration cycling involves non-proportional loading instead of proportional loading, and thermal effects may cause material property migration and microstructure evolution in the solder material ([11]Basaran and Chandaroy, 1998).

In this project, concurrent thermal cycling and vibration tests are conducted to explore the cyclic behavior of solder joints and plasticity occurred in vibration coupled with thermal cycling in solder joint fatigue life. Realistic BGA packages are used for testing. High sensitivity Moiré interferometry (MI) method is used to capture the in-plane deformation field of entire specimen cross-section with submicron resolution. MI has been used for studying thermal mechanical behavior ([15]Han and Guo 1995, [16]Zhu and Liu 1997, [17]Han 1997, [18]Wang et al. 1998, etc., [19]Zhao et al. 1999a). MI is used here to measure the cyclic inelastic deformation fields.

Specimen Preparation

The BGA package used for testing is cut through the center of a row of solder balls, and the cross-section is shown in Figure 1. It has a multilayered structure; with three major layers connected by two layers of BGA solder joints. All the solder joints are Sn63/Pb37 eutectic solder alloy. The solder joints selected for the measurement of the thermal response are at the bottom layer, totally 30 joints in each row, which bonds the FR4 PCB layer and polymer connector layer. These solder joints have been observed to be the most vulnerable interconnections of the entire device under thermal loading due to the significant thermal expansion mismatch between the two layers. Additionally, there are tiny copper foils inserted in the polymer connector layer, which are the pads for the solder joints.

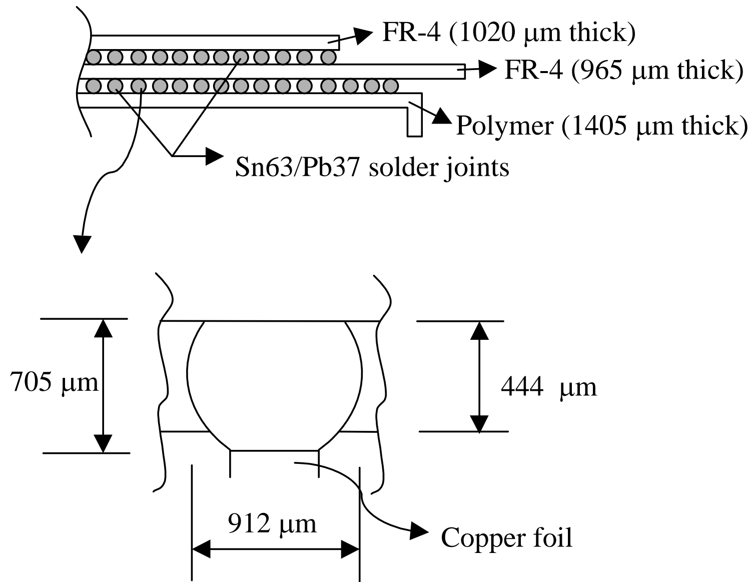

Figure 1 Specimen Profile

Specimen surface is first polished flat, cleaned with acetone, and dried thoroughly. Specimen grating is transferred from a grating mold using a layer of epoxy. To distinguish each solder joint without filling up the gap between the joints, a thin layer of epoxy is wiped onto the specimen surface using a piece of optical tissue. The double layers of aluminum coating are applied to the grating mode to ensure the smooth separation of the specimen and grating mode in the replication procedure.

The specimen was cut by a high precision diamond wheel saw right through the center of the solder joints of interest. The exposed cross section was then polished by using abrasive papers with different grain sizes. The surface was then cleaned and dried thoroughly and ready for diffraction grating replication. Probably one of the most important parts of this project was selection of the epoxy. A special type of epoxy was chosen after years of trial and errors to make sure that the specimen grating would stand the peak cycling temperature for many cycles. It should be pointed out that this is the first time in the published literature Moiré Interferometry has ever been used for fatigue life experiments under combined loading. Only other study ever published on using Moiré Interferometry for cycling loading is by Han (1997). In the latter study the author was able to cycle the specimen four cycles without damaging the optical grating on the specimen. On the other hand using the grating replication technology developed in this study a

specimen can be cycles until failure without any degradation in the grating. The epoxy used here has a very low viscosity to achieve a very thin layer as it was spread out on the specimen surface to replicate the grating. The two-component epoxy was fully mixed and sent to a vacuum chamber for degas. After degassing, the epoxy was spread carefully on the specimen surface, and a master grating was stamped onto the surface. The specimen and master grating pair were kept tightly compressed against each other until the end of the epoxy-curing period. The specimen was then separated from the master grating with the replicated diffraction grating on its surface. It is important to control the degas procedure to be completed in a certain amount of time so that enough time is left for replication before the epoxy working life limit is reached. The grating used in this project is 1200 lines/mm.

Moiré Interferometry

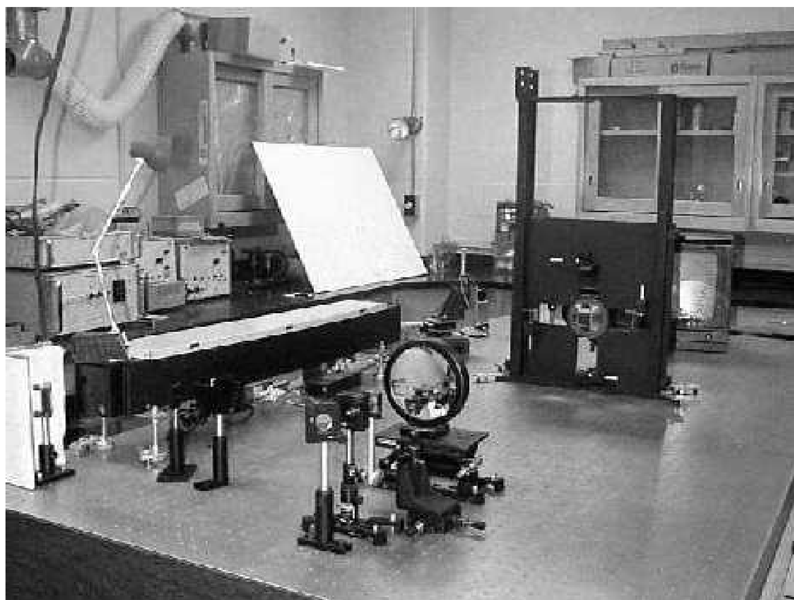

Figure 2 Optical table

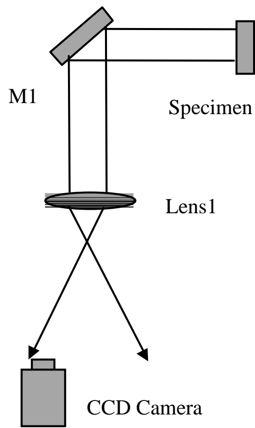

Figure3 (a) Imaging System 1

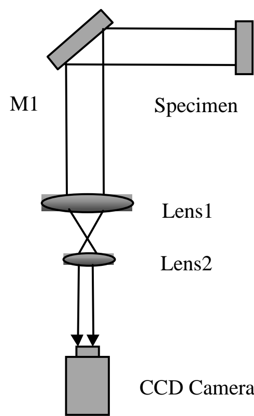

Figure3 (b) Imaging System 2

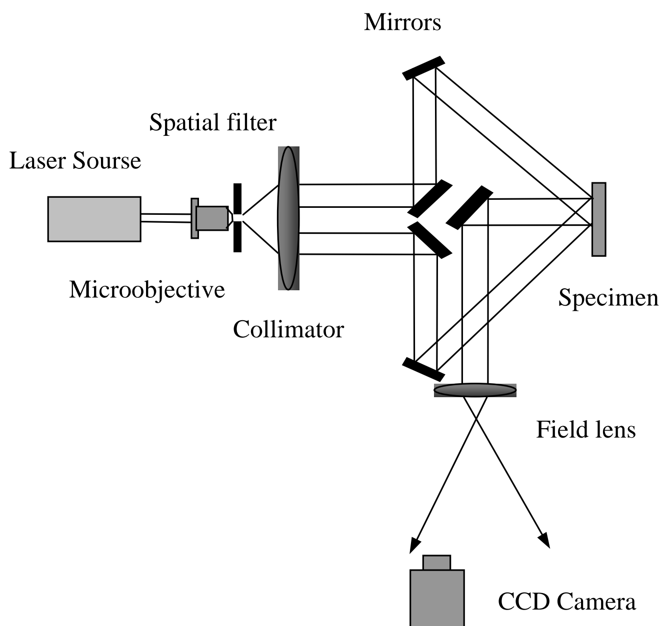

(c) Top view of the setup

Figure 3 Optical setup of Moiré Interferometry

Moiré Interferometry setup used here is similar to the one used earlier by [19]Zhao et al. (1999a). The optical table of MI is shown in Figure 2. The interferometry layout is shown in Figure 3. Each two beams, generated from the same single laser source, lie in the same plane to create an interferometry pattern. U-field is referred to the fringe field generated by the two beams in the horizontal plane and V-field denotes

the fringe field generated by the vertical two beams. The fringe contour represents the equal deformation points, and each fringe is given an order number. Increasing of the order number with regard to a reference order number represent increasing of deformation from the reference point. The relationships between the fringe order and actual in-plane deformation is given by [20]Post et al (1994):

$$U = \frac{Nx}{f} \quad (1)$$

$$V = \frac{Ny}{f} \quad (2)$$

Where, U is the displacement in the x direction; V is the displacement in the y direction; and f = 2fs, where fs is the frequency of the specimen diffraction grating. In this study, fs=1200 lines/mm; Nx is the horizontal fringe order, and Ny is the vertical fringe order. Differentiation of the displacement with respect to the two basic directions: horizontal (x) and vertical (y) gives the strain equations:

$$\varepsilon_x = \frac{\partial U}{\partial x} = \frac{1}{f}\left[\frac{\partial N_x}{\partial x}\right] \quad (3)$$

$$\varepsilon_y = \frac{\partial V}{\partial y} = \frac{1}{f}\left[\frac{\partial N_y}{\partial y}\right] \quad (4)$$

$$\gamma_{xy} = \frac{\partial U}{\partial y} + \frac{\partial V}{\partial x} = \frac{1}{f}\left[\frac{\partial N_x}{\partial y} + \frac{\partial N_y}{\partial x}\right] \quad (5)$$

Imaging System

Two imaging systems have been used to capture different types of images as shown in Figure 2. The first imaging system is used to capture the enlarged image of individual solder joints to observe detailed local deformation. A plane mirror (M1) and a field lens (Lens1) are the main components in system1. The

plane mirror is to direct the imaging beam to the CCD camera, and field lens is to collect the beam and enlarge the image. The CCD camera was mounted on a 3D mechanical translator, so that its position can be adjusted precisely. Especially, in the horizontal direction, enough free path is provided so that the CCD camera can capture each solder joint of interest by moving along the free path. The field lens needs to be big so that the imaging beams can be as centered as possible to avoid image distortion and to obtain the best quality of the image.

The second imaging system is used to capture the image of the entire specimen to give a global view of the deformations in all solder joints. For this purpose, another short focal-length lens (Lens2) is added to focus the entire image so that the whole image just fits in the area array of the photo detectors of the CCD camera. The light-intensity is reduced in this case to prevent saturation of the CCD. Saturation turns the image into a field of white noise.

Concurrent Vibration and Thermal Cycling

The concurrent test is conducted using an environmental loading unit consisting of a Super AGREE thermal chamber with ramping capability of 30°C/min and an Unholtz-Dickie electrodynamic shaker, which can apply 100g maximum acceleration in vibration and 300g maximum acceleration in shock. The assemblage for concurrent test is shown in Figure 4. Specimen is fixed in a testing fixture as shown in Figure 5. Before testing the undeformed specimen grating is used to tune the optical setup to a null field. The optical setup is then kept in the aligned manner until testing ends. The specimen is then taken to the loading unit to perform cycling. At the end of cycles, the specimen is taken out, and the plastic deformation at that stage is measured using the MI, and the optical fringe field is digitally recorded on a computer. After measurement it is put back for further cycling.

Figure 4 Concurrent testing units

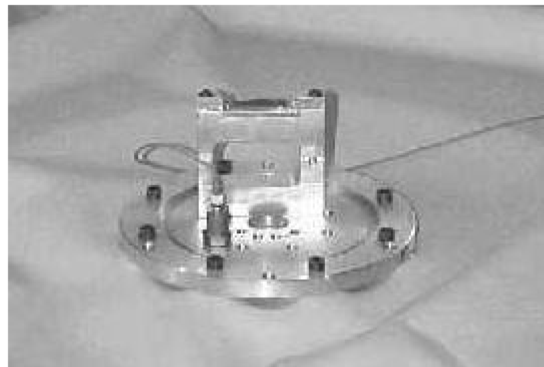

Figure 5 Specimen and the fixture on the shaker armature

The load profile is shown in Figure 6 and 7. Temperature range is -55 °C to 125 °C, with ramping rate of 20 °C/min, dwelling time of 12 min at highest and lowest temperature respectively, and total cycle period 42 min. The coupled vibration has frequency of 100 Hz and acceleration of 50 g.

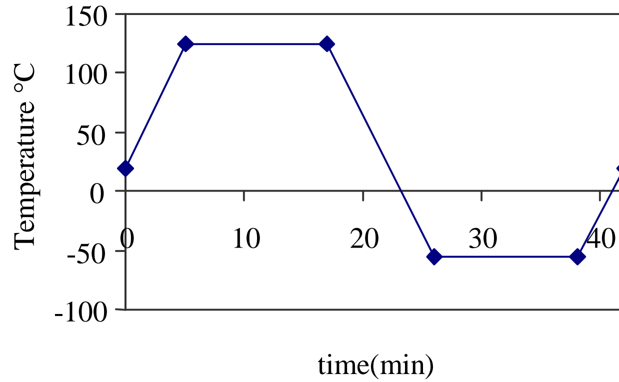

Figure 6 Temperature history

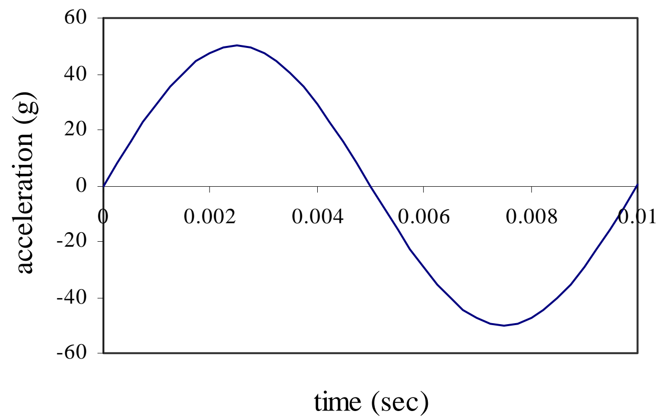

Figure 7 Vibration load profile

Results and Discussion

Figure 8a and 8b shows the MI fringe pattern of the deformation fringe field after the 1st combined loading cycle. The irreversible shear strain distribution of the observed row of solder joints is shown in figure 9. The largest strain occurs at the free edge joint #1. Inner joints show smaller value of irreversible shear strain. This deformation trend is in agreement with thermal cycling results ([19]Zhao et al. 1999a), and is also discussed using FEM ([21]Basaran and Zhao, 1999). It is obvious that free edge joints will yield first

as shear stress and strain developed from the free edge joint towards inner ones. Debonding or fracture may occur at the edge solder joint.

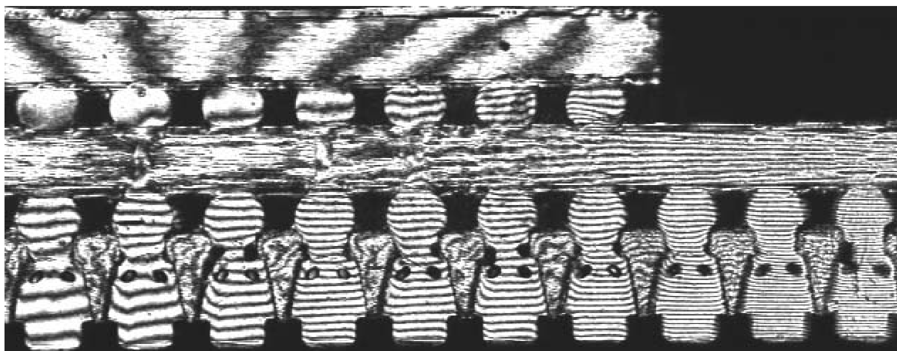

Figure 8a U-field of deformation fringe patterns
After the 1st combined loading cycle

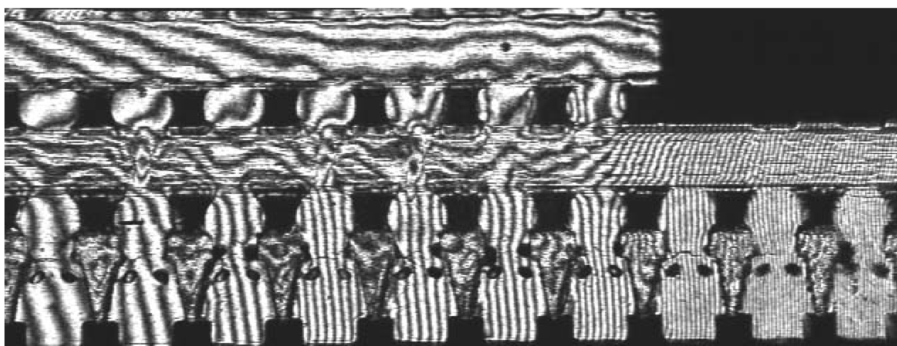

Figure 8b V-field of deformation fringe patterns
After the 1st combined loading cycle

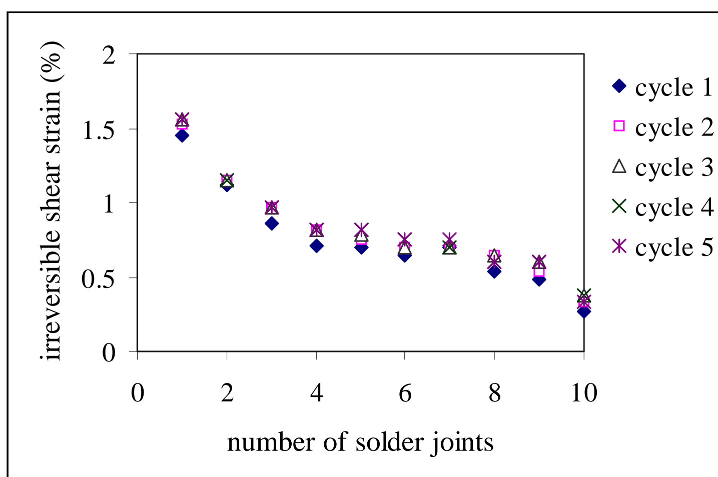

Figure 9 Irreversible shear strain vs. solder joint number

The calculated total average irreversible shear strains at the end of a certain number of thermal cycles are plotted in Figure 10 for joint1, joint2, joint3, jont5, joint6 and joint9. It can be seen that the fastest increment of the irreversible shear strain is induced in the first cycle. As the number of cycles increases, the amount of the increment of plastic deformation in each cycle is reduced. This curve shows that using Coffin-Manson curves for combined environment fatigue life yields inaccurate estimation of the fatigue life of micron scale solder joints where the ratio of total volume to a single colony volume is relatively small, less than 20. According to Coffin-Manson curve on fatigue, cyclic plastic strain increases linearly from cycle to cycle. Researchers have shown validity of Coffin-Manson relation for bulk materials. But this test shows that it is invalid for small-scale systems, such as in microelectronics. This plateau trend in the shear strain vs. the number-of-cycles curve is similar to thermal cycling testing ([19]Zhao, et al. 1999a). Virtually every solder joint presents this characteristic. This demonstrates the stabilization process in cyclic loading and is in line with findings reported by [11]Basaran and Chandaroy (1998), where the authors analytically show that damage accumulation is not linear.

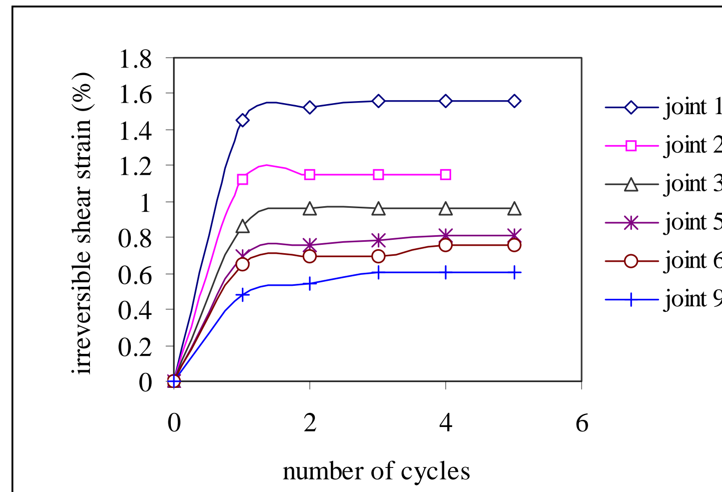

Figure 10 Irreversible shear strain vs. number of thermal cycles

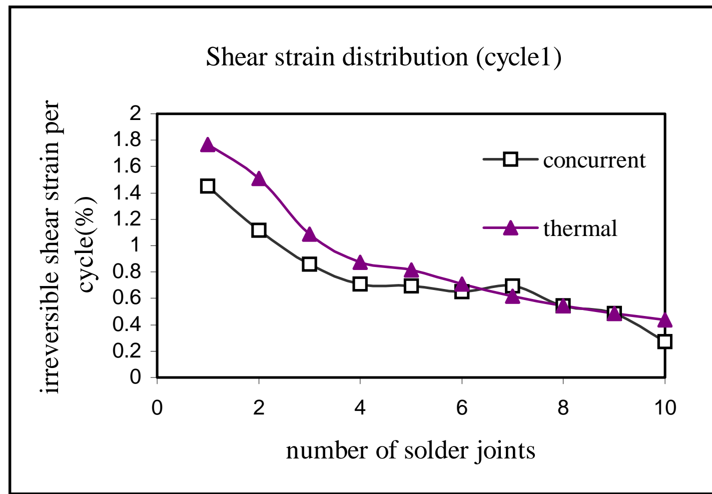

Figure 11 Cycle 1 irreversible shear strain vs. solder joint number

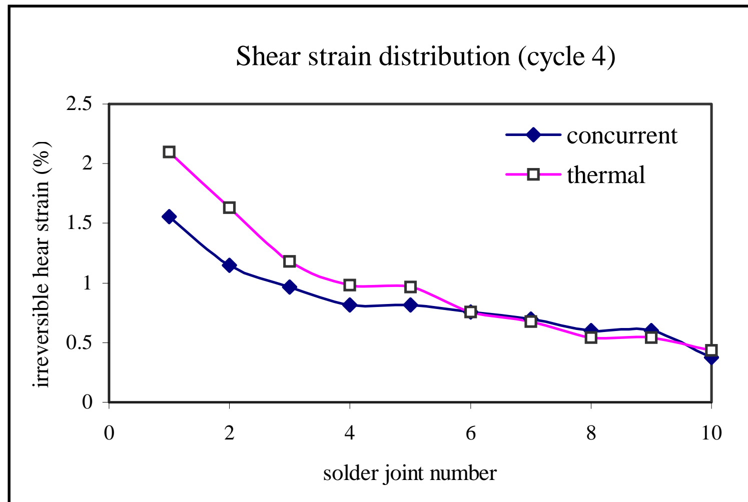

Figure 12 Cycle 4 irreversible shear strain vs. solder joint number

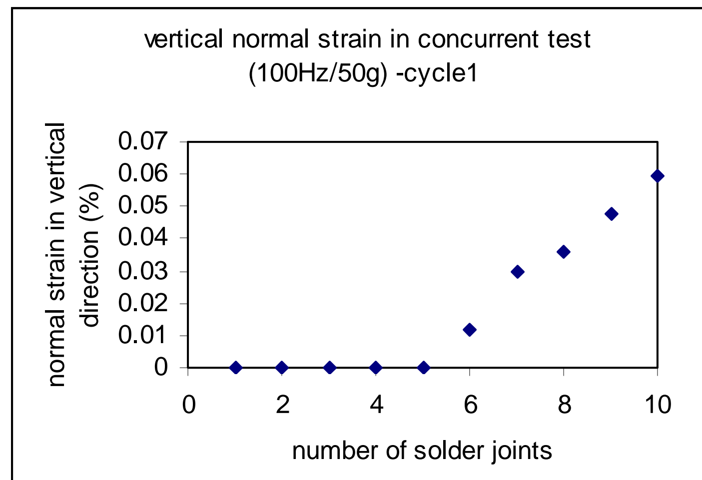

Figure 13 Cycle 1 irreversible peeling (normal) strain vs. solder joint number

Comparison with Thermal Cycling Alone

As shown in figure 11, the average plastic strain at the end of the first cycle under concurrent loading is compared to the results obtained from pure thermal cycling test with the same temperature profile ([19]Zhao et al. 1999a). In figure 12, the irreversible shear strain distribution curves obtained from the two loading conditions are also plotted for the 4th cycle. These two figures show that concurrent loading induces less irreversible shear strain than thermal loading alone. This phenomenon inferred that vibration has significant effect on the inelastic behavior of solder joints, especially coupled with thermal cycling. Vibration response at room temperature is close to elastic, and plastic response is obvious at elevated temperature as shown in [22]Zhao et al. (1999b). The response under concurrent thermal and vibration cannot be explained by simple superposition of thermal cycling and dynamic cycling strains or stresses.

The two figures above show that irreversible shear strain at the end of cycles is smaller in the concurrent loading case than that in the pure thermal cycling case. It seems that dynamic force, which is reversing in a high frequency, confines the joint, which in turn restricts the creep, flow mechanism, and thus reduces the overall cyclic plastic strain range. However, as one can imagine, a large number of mini-cycles are imposed on a large thermal cycle. The total plastic energy dissipated during concurrent cycling could still be larger as creep cannot be ignored during low frequency high temperature vibration ([22]Zhao et

al. 1999b). The plastic energy dissipated in these mini-cycles can vary according to different values of vibration frequency and acceleration, [11]Basaran and Chandaroy (1998) Figure 13 shows the irreversible normal strain (vertical) distribution among solder joints for concurrent loading for the 1st cycle only. Due to the boundary conditions imposed on the BGA package further cycling does not generate more strain in the solder joints that is large enough to be detected by the sub-micron resolution. In other frequency and acceleration cases, normal strain is too small to be detected by the resolution, i.e., they are all far bellow one fringe. The boundary conditions used in the test are identical to the actual field use.

Another point of view to explain smaller irreversible strain in concurrent loading is the theory of thermodynamics. It is widely accepted that irreversible strain is related to degradation (damage) in a system. [23]Basaran and Yan (1998) developed a damage evolution equation based on the second law thermodynamics. In their model Basaran and Yan (1998) have shown that starting with the entropy – disorder relation proposed by Boltzman (1898)

$$s = k \ln w$$

(6)

Where s is the entropy of the system, k is Boltzman constant and w is disorder parameter and linking this definition of entropy with the Helmholtz free energy equation,

$$\phi = e - \theta s$$

(7)

Where e is the internal energy, θ is the absolute temperature and s is the entropy, the following damage evolution equation can be obtained, [assuming that entropy production is non-negative for solid damage mechanics problems]

$$D = 1 - e^{-\frac{\Delta e - \Delta\phi}{N_0 k\theta / \overline{m}_s}}$$

(8)

$$\Delta e - \Delta\phi = \frac{1}{\rho}\left(\int_{\varepsilon_o}^{\varepsilon} \sigma_{ij}\, d\varepsilon_{ij}^{in}\right) - \int_{t_o}^{t} \frac{1}{\rho}\frac{\partial q_i}{\partial x_i} dt + \int_{t_o}^{t} \dot{\gamma}\, dt$$

(9)

Where, D is a measure of damage in the system, ρ is mass density, σ_{ij} total stress tensor, ε_{ij}^{in} inelastic strain tensor, θ denotes absolute temperature in Kelvin, $\dot{\gamma}$ is the distributed internal heat production rate per unit mass, q_i is the heat flux tensor, N_o is Avagadro's constant, k is Boltzman's constant, $\overline{m}_s$ is the specific mass and dt is the time increment. It is obvious from equation (7) that at higher temperature more plastic energy dissipation is needed to cause the same amount of damage due to heat flux. In Eq. (7) first and third terms are energy dissipated by inelastic work and heat dissipated due diffusion, respectively. The second term is the energy pumped into the system by heat flux. This latter energy component has an opposite effect compared to two other energy components in Eq. (7). When there is heat flux coming into the system damage due to inelastic work is reduced. This thermodynamic damage evolution relation probably explains the testing result obtained in our testing and the results obtained by [8]Upadhyayula and Dasgupta (1997), where room temperature shock vibration causes shorter fatigue life than concurrent vibration and thermal cycling. From the material property migration point of view, solder joint exhibits more brittle behavior at room temperature than at elevated temperature. Same vibration can induce much higher stress in the solder joint at room temperature than at higher temperature.

Cyclic Stabilization

The irreversible strains vs. number-of-cycles curves are plotted in Figure 14 for pure thermal cycling and concurrent thermal-vibration cycling loading cases. It is obvious that the irreversible shear strain per cycle tends to stabilize as the number of cycles increases. However, in the latter case, this stabilization process is about 2 cycles, much faster than the former case where it is about 8 cycles. This is probably related to the effect of straining to microstructure stabilization, which in turn related to the stabilization of flow behavior of eutectic solder alloy at high temperature. In Figure 14 concurrent loading strains are plotted up to five cycles due to the fact that there is no change in the slope of the curve and also this is a very expensive experiment to run.

The as-cast eutectic Pb/Sn solder joint is microstructurally unstable, and exhibits unstable flow behavior during the first few cycles. Approaching to an asymptotic value of irreversible strain per cycle represents the stabilization. After that, microstructure will still evolve, but in a much slower pace as discussed by [24]Kashyup and Murty (1982). It is well known that straining Pb/Sn solder yields stable microstructure. In vibration coupled with thermal cycling condition, the solder material is strained much faster by a dynamic force back and forth in a high frequency, which contributes to the faster stabilization of solder microstructure, [11]Basaran and Chandaroy (1998).

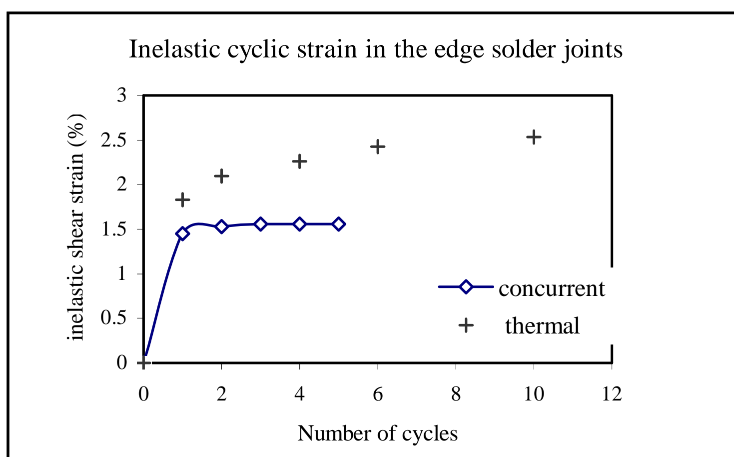

Figure 14 Irreversible shear strain vs. number of thermal cycles for thermal only and concurrent loading.

Conclusions

To study the contribution of vibration to thermal fatigue life of microelectronics solder joints, a series of concurrent thermal cycling and vibration tests are conducted on real life BGA packages. The cyclic behavior of solder joints in vibration coupled with thermal cycling is recorded and compared with pure thermal cycling results. High sensitivity Moiré interferometry has been successfully applied to capture the in-plane deformation field of specimen cross-section with sub-micron resolution.

Test results show that, although thermal cycling induced deformations dominate the overall response, vibration significantly modifies the total behavior of solder joints in the concurrent loading. Test results also indicate that Miner's rule is not accurate for concurrent environment due to its lack of consideration of thermal and vibration interaction and scale effect.

The cyclic behavior of solder joints is reflected in the stabilization of cyclic inelastic strain. This behavior is possibly related with microstructure evolution process of the eutectic solder joints, and vibration contributes to such evolution process by straining the material in a faster pace.

Test results obtained here contradict established and proven mechanics rules, such as Miner's rule and Coffin-Manson, for bulk materials where member dimensions are very large compared to a single grain or colony size, This contradiction is probably due to the scale effect. Similar result were recently also reported by [25]Hutchinson (2000).

Tests described here are aimed at better understanding of material behavior of actual solder joints under realistic thermal and vibration loading and providing a solid basis for more accurate material modeling and fatigue life prediction.

Acknowledgments

The Department of Defense Office of Naval Research Young Investigator Award to Prof. Basaran sponsors this research project. Helpful discussions with Dr. Roshdy Barsoum, Director of Solid Mechanics Program at ONR, are gratefully appreciated.

References

1. Steinberg, D.S., *Vibration Analysis for Electronic Equipment*, 2nd ed., John Wiley & Sons, New York, 1988.
2. Lau, John H. and Donald W. Rice, "Solder Joint Fatigue in Surface Mount Technology: State of the Art", Solid State Technology, pp.91-104, Oct. 1985.
3. Blanks, H.S., "Accelerated Vibration Fatigue Testing of Leadless and Solder Joint", Microelectronics and Reliability, Pergoman Press, UK, Vol. 15, p.213-219, 1976.
4. Markstein, H.W., "Designing Electronics for High Vibration and Shock", Electronic Packaging & Production, pp.40-43, April 1987.
5. Suhir, E. and Lee, Y.C., "Thermal, Mechanical, and Environmental Durability Design Methodologies", Vol.1 in Electronic Material Handbook, ASM International, New York, 1998.
6. Barker, D.B and Sidharth, K., "Vibration Induced Fatigue Life Estimation of Corner Leads of Peripheral Leaded Components", Proceedings, ASME International Mechanical Engineering Congress and Exposition, ASME, New York.
7. Darbha, K., Ling, S., Upadhyayula, K. and Dasgupa, A., "Stress Analysis of Surface-Mount Interconnects Due to Vibrational Loading", paper presented at the ASME International Mechanical Engineering Congress and Exposition, Atlanta, GA, 1996.
8. Upadhyayula, K. and Dasgupta, A., "An Incremental Damage Superposition Approach for Reliability of Electronic Interconnects Under Combined Accelerated Stresses", ASME International Mechanical Engineering Congress & Exposition, Dallas, Texas, Nov.16-21, 1997.
9. Chandaroy, R. and Basaran, C., "Damage Mechanics of Surface Mount Technology Solder Joints Under Concurrent Thermal and Dynamic Loading", Journal of Electronic Packaging, Vol.121, p.61-68, June 1999.

10. Barker, D., Vodzak, J., Dasgupta, A. and Pecht, M., "Combined Vibrational and Thermal Solder Joint Fatigue- A Generalized Strain Versus Life Approach", Journal of Electronic Packaging, Vol. 112, p.129-134, June1990.
11. Basaran, C. and Chandaroy, R., "Mechanics of Pb40/Sn60 Near Eutectic Solder Alloys Subjected To Vibrations", Applied Mathematical Modeling, 22, pp.601-627, 1998.
12. Busso, E. P., Kitano, M. and Kumazawa, T., "A Visco-Plastic Constitutive Model for 60/40 Tin/Lead Solder Used In IC Package Joints", Journal of Engineering Materials and Technology, July 1992, Vol.114, p.331-337, 1992.
13. Skipor, A. F., Harren, S. V. and Botsis, J., "On the Constitutive Response of 63/37Sn/Pb Eutectic Solder", Journal of Engineering Materials and Technology, Vol.118, p.1-11, Jan., 1996.
14. Bonda, N.R. and.Noyan, I.C., "Effect of the Specimen Size in Predicting the Mechanical Properties of PbSn Solder Alloys", IEEE transactions on CPMT, pp.208-212, June 1996.
15. Han, B. and Guo, Y. "Thermal Deformation Analysis of Various Electronic Packaging Products by Moiré and Microscopic Moiré Interferometry", Journal of Electronic Packaging, Vol. 117, p.185-191, Sep. 1995.
16. Zhu, J. and Liu, S.,"Thermal Deformation And Stress Analysis Of A Column Grid Array Package By Hybrid Moiré/FEM Method", ASME International Mechanical Engineering Congress & Exposition, Dallas, Texas, Nov. 16-21, 1997.
17. Han, B. "Deformation Mechanism of Two-Phase Solder Column Interconnections Under Highly Accelerated Thermal Cycling Condition: An Experimental Study", Journal of Electronic Packaging, Vol. 119, p.189-196, Sep. 1997.
18. Wang, J., Qian, Z., Zou, D, and Liu, S. "Creep Behavior of a Flip-Chip Package By Both FEM Modeling And Real Time Moiré Interferometry", Journal of Electronic Packaging, Vol. 120, p.179-185, June 1998.

19. Zhao, Y., Basaran, C., Cartwright, A. and Dishongh, T., "Thermomechanical Behavior Of Micron Scale Solder Joints: An Experimental Observation", Journal of the Mechanical Behavior of Materials, Vol.10, No.3, p.135-146, 1999a.

20. Post, D., Han, B. and Ifju, P. *High Sensitivity Moiré*, Springer-Verlag, 1994.

21. Basaran,C. and Zhao,Y., "Closed Form vs. Finite Element Analysis of Laminated Stacks", International Journal of Finite Elements in Analysis & Design, 32, 1999, 163-179.

22. Zhao, Y., Basaran, C., Cartwright, A. and Dishongh, T., "Thermomechanical Behavior Of Micron Scale Solder Joints Under Dynamic Loads", Mechanics of Material, 32, 2000,161-173.

23. Basaran, C., and Yan, Y.," A Thermodynamic Framework for Damage Mechanics of Solder Joints," Trans. of ASME Journal of Electronic Packaging, v 120 n 4, p379-384, Dec. 1998.

24. B.P.Kashyap and G.S.Murty, "Superplastic Behavior of the Sn-Pb Eutectic in the As-Worked State", Metallurgical Transactions A, Vol. 13A, pp.53-58, Jan. 1982.

25. Hutchinson, J.W. “Plasticity at Micron Scale,” Int. J. of Solids and Structures, 37 (2000) 225-238.

26. Boltzman, I., (1898) Lectures on Gas Theory, Univ of California Press, Berkeley, CA (Translation by S. Brush, 1964).

27. Wei, Y., Chow, C.L., Fang, H.E., and Nielsen, M.K., 1999, “Characteristics of creep damage for 60Sn-40Pb solder material,”ASME 99-IMECE/EEP-15